Applied Catalysis B: Environmental 176–177 (2015) 731–739

Contents lists available at ScienceDirect

Applied Catalysis B: Environmental

journal homepage: www.elsevier.com/locate/apcatb

On the deactivation of Mo/HZSM-5 in the methane dehydroaromatization reaction

Christiaan H.L. Tempelman, Emiel J.M. Hensen *

Laboratory of Inorganic Materials Chemistry, Schuit Institute of Catalysis, Eindhoven University of Technology, Den Dolech 2, 5612 AZ Eindhoven, The Netherlands

ARTICLE INFO

Article history:
Received 22 December 2014
Received in revised form 21 April 2015
Accepted 24 April 2015
Available online 25 April 2015

Keywords:
Methane
Aromatization
Mo/HZSM-5
Deactivation
Coke

ABSTRACT

The deactivation of Mo/HZSM-5 during the non-oxidative methane aromatization (MDA) reaction that yields benzene and hydrogen was investigated. Catalysts were recovered from the reactor after pre-activation and after increasing time on stream in methane. The physico-chemical properties of the spent catalysts were characterized in detail by Ar physisorption, ^{27}Al MAS NMR and X-ray photoelectron spectroscopy. The nature of the carbon deposits was determined by UV Raman spectroscopy and TGA, and the size and location of the Mo-carbide particles by TEM and STEM-HAADF. The results show that the main cause for catalyst deactivation is the formation of a carbonaceous layer at the external zeolite surface. This layer is made up from polyaromatic hydrocarbons and decreases the accessibility of the Brønsted acid sites in the micropores. At the same time, the decreased interaction of the Mo-carbide particles with the external zeolite surface results in their sintering. The lower Mo-carbide dispersion decreases methane conversion rates. The decreased accessibility of the Brønsted acid sites shifts the selectivity from benzene to unsaturated intermediates formed on the Mo-carbide particles. Silylation of the external surface mainly results in lower rate of coke formation at the external surface, slowing down catalyst deactivation.

1. Introduction

Dwindling fossil resources and concerns about the effect of their combustion on our climate add urgency to the replacement of these non-renewable resources by renewable ones. For example, to surpass petroleum as the main resource for aromatics scientists explore the use of biomass as alternative feedstock [1]. A general problem is that the conversion technologies for renewable resources such as biomass and solar energy are often at an early stage of development. Usually, the development from the discovery of a novel energy technology to large-scale commercial implementation takes decades [2]. Accordingly, transition technologies based on relatively clean feedstock such as natural gas are increasingly considered to fill the gap between conventional oil and coal based and future sustainable processes. In energy scenarios, the abundance of natural gas is evident with estimated reserves of 180 trillion ton cubic meters [3]. New technologies to extract natural gas from shale rock are already leading to drastic changes in the energy and chemicals industry at the global scale [1,4]. On the other hand, a significant fraction of the natural gas reserves is located in remotely located fields. Because of the small size of many of these fields, investments in capital intensive transportation via pipelines or liquefaction are often not justified. For similar reasons, it is common practice to flare associated gas from oil production in order to meet safety and environmental legislations. Chemical conversion toward high-value fuels and chemicals would be an alternative to make recovery of these natural gas resources economically more attractive.

Currently, catalytic steam and autothermal reforming and gasification are common technologies to convert natural gas into synthesis gas; synthesis gas serves as the platform for the manufacture of a wide range of chemicals. The CAPEX and OPEX for the syngas production step are very high, so that it is only profitable to construct large plants. Accordingly, it remains a strong desire of the chemical industry to develop a simple process to upgrade natural gas to liquids. One such process may be the direct aromatization of methane to benzene under non-oxidative conditions (methane dehydroaromatization, MDA). Benzene is an attractive intermediate, because it can be more easily transported than natural gas. In addition, the increasing use of ethane from wet shale gas instead of naphtha to produce ethylene is putting pressure on the aromatics supply. Direct methane to aromatics conversion would be very desirable in this context [1].

* Corresponding author. Tel.: +31 40 2475178.
E-mail address: e.j.m.hensen@tue.nl (E.J.M. Hensen).

http://dx.doi.org/10.1016/j.apcatb.2015.04.052
0926-3373/

Methane dehydroaromatization was first discussed by Wang et al. in 1993 [5]. Mo/HZSM-5, the most common catalytic material for this reaction, is a bifunctional catalyst. The molybdenum carbide phase is formed during carburization of the initial molybdenum oxide phase. It converts methane into ethylene, while Brønsted acid sites in the shape-selective micropores of HZSM-5 zeolite convert ethylene to benzene and other aromatics. The process is typically operated at temperatures higher than 873 K because of the low reactivity of methane. Thermodynamic equilibrium limits the reaction. In principle, higher reaction temperatures than the most frequently reported one (973 K) result in higher benzene yield, but also lead to rapid carbon laydown on the catalyst. The formation of coke, which causes relatively fast deactivation of the catalyst, is the main challenge in the development of a commercial process for methane dehydroaromatization [6].

Several studies have attempted to elucidate the reasons for the rapid deactivation of Mo/HZSM-5 catalysts during the MDA reaction [7–17]. Extensive formation of polyaromatics hydrocarbon carbon deposits was identified as the main reason for catalyst deactivation. The formation of this type of carbon is assumed to take place at the Brønsted acid sites (BAS) located on the external surface of the zeolite crystals [13,14]. Some authors suggested that such carbon species may eventually block the micropore apertures [7,8]; this would explain the increased formation of ethylene at the expense of benzene [9]. Deactivation of the external surface BAS by silylation has been shown to decrease to some extent the formation rate of such unwanted carbon species, but catalyst deactivation cannot be completely prevented in this way [15–17]. Therefore, the coverage of the BAS inside the micropores by carbonaceous species is also considered to contribute to catalyst deactivation [10]. We have recently reported that silylation after Mo introduction yields better MDA catalysts than Mo introduction after zeolite silylation [17].

Improvements of the MDA process may involve improved catalyst technology but also reactor engineering approaches to cope with rapid catalyst deactivation. Such developments will strongly hinge on better insight in the deactivation of the catalyst. In the present study, we have investigated in detail the different stages in the life of a Mo/HZSM-5 catalyst during methane dehydroaromatization. The precursor activated and deactivated catalysts after different times on stream were extensively characterized for their physical and chemical properties. The obtained results are captured in a model that describes deactivation during the MDA reaction.

2. Experimental

2.1. Catalyst synthesis

The proton form of ZSM-5 (Alsi-Penta) was obtained from Süd-Chemie (now Clariant). The starting material had a Si/Al ratio of 15 as determined from ICP-AES elemental analysis. For Mo loading, the zeolite was impregnated (incipient wetness impregnation) with an aqueous solution of ammonium heptamolybdate tetrahydrate (AHM, Merck). The target Mo content was 6 wt%. After impregnation, the material was dried for 1 h at room temperature followed by calcination in artificial air at varying temperatures and for varying dwell times after heating to the final temperature at a rate of 1.5 K/min. Molybdenum modified zeolites are denoted by Mo/HZSM-5.

A portion of the molybdenum modified zeolite was silylated following a method adapted from Ding et al. [14]. Typically, 2 g of zeolite was dried overnight at 373 K and then dispersed in 50 ml *n*-hexane. To the suspension, an amount of 0.3 ml tetraethyl orthosilicate (TEOS, Merck) was added and stirred for 1 h under reflux. The amount of TEOS added corresponds to 0.4 wt% based on the amount of zeolite in the suspension. The treated zeolite was then filtered off and dried overnight at 373 K. The resulting zeolite was calcined by a two-step procedure in artificial air. The first step consisted of heating the sample at a rate of a 2 K/min to 393 K followed by an isothermal period of 2 h. In the second step the temperature was increased to 773 K at a rate of 0.2 K/min followed by an isothermal period for 4 h. The silylated Mo/HZSM-5 is denoted as Mo/HZSM-5(Si).

2.2. Characterization

The Mo and Al content of the zeolites was determined by inductively coupled plasma optical emission spectroscopy (ICP-OES, Spectro CIROS CCD spectrometer). Prior to ICP measurements, the zeolite samples were dissolved in a mixture of $HF/HNO_3/H_2O$ (1:1:1).

UV Raman spectra were recorded with a Jobin–Yvon T64000 triple stage spectrograph with a spectral resolution of 2 cm^{-1}. The 244 nm line at of a Lexel 95-SHG laser was used as the excitation source. The power of the laser on the sample was about 2 mW.

Magic angle spinning (MAS) ^{27}Al single pulse NMR spectra were recorded on a Bruker Avance DMX-500 NMR spectrometer (11.7 T; the Al resonance frequency at this field is 130.3 MHz). A 2.5 mm MAS probe head was used. The ^{27}Al chemical shift was referenced to a saturated $Al(NO_3)_3$ solution. In a typical experiment, 10 mg of well-hydrated sample was packed in a 2.5 mm zirconia rotor. The MAS sample rotation speed was 20 kHz. ^{27}Al NMR spectra were recorded with a single pulse sequence with 180° pulse duration of 1 μs and a interscan delay of 1 s.

Argon sorption isotherms were measured at 87 K on a Micromeritics ASAP2020 system in static measurement mode. The samples were outgassed at 623 K for 8 h prior to the sorption measurements. The Brunauer–Emmett–Teller (BET) equation was used to calculate the specific surface area (S_{BET}) in the pressure range $p/p_0 = 0.05 - 0.25$. The mesopore volume (V_{meso}) and mesopore size distribution were calculated using the Barrett–Joyner–Halenda (BJH) method on the adsorption branch of the isotherm. The micropore area (S_{micro}) and micropore volume (V_{micro}) were calculated from the *t*-plot curve using the thickness range between 3.5 and 5.4 Å [19].

Transmission electron micrographs were obtained with a FEI Tecnai 20 instrument at an electron acceleration voltage of 200 kV. Typically, a small amount of sample was suspended in ethanol, sonicated and dispersed over a Cu grid with a holey carbon film.

Weight-loss curves were obtained from thermogravimetric analysis (TGA) using a Mettler Toledo TGA/DSC 1 apparatus. Samples were heated in uncovered alumina crucibles at a rate of 5 K/min to 1023 K in a 2/1 (v/v) He/O_2 flow.

Isotopic H/D exchange between C_6H_6 and C_6D_6 was carried out in a 10-channel parallel microflow reactor setup. Typically, 50 mg of zeolite was loaded in each quartz tubular reactor with an internal diameter of 4.0 mm. Zeolites were first pelletized and then crushed and sieved in a 125–250 μm mesh fraction. The ten quartz tubes with the catalyst contained between quartz wool plugs were then placed in the parallel reactor setup. Before reaction samples were dehydrated in a He flow to 723 K at a rate of 5 K/min followed by an isothermal period of 6 h. After cooling to 303 K, the reaction was started by switching the reactor feed to the gas flow containing a 90/10 (v/v) C_6H_6/C_6D_6 mixture. The effluent products were analyzed by mass spectrometry. The rate of H/D exchange was determined as a function of temperature.

2.3. Catalytic activity measurements

An amount of 0.5 g of catalyst was introduced in a tubular quartz reactor with a length of 490 mm and an internal

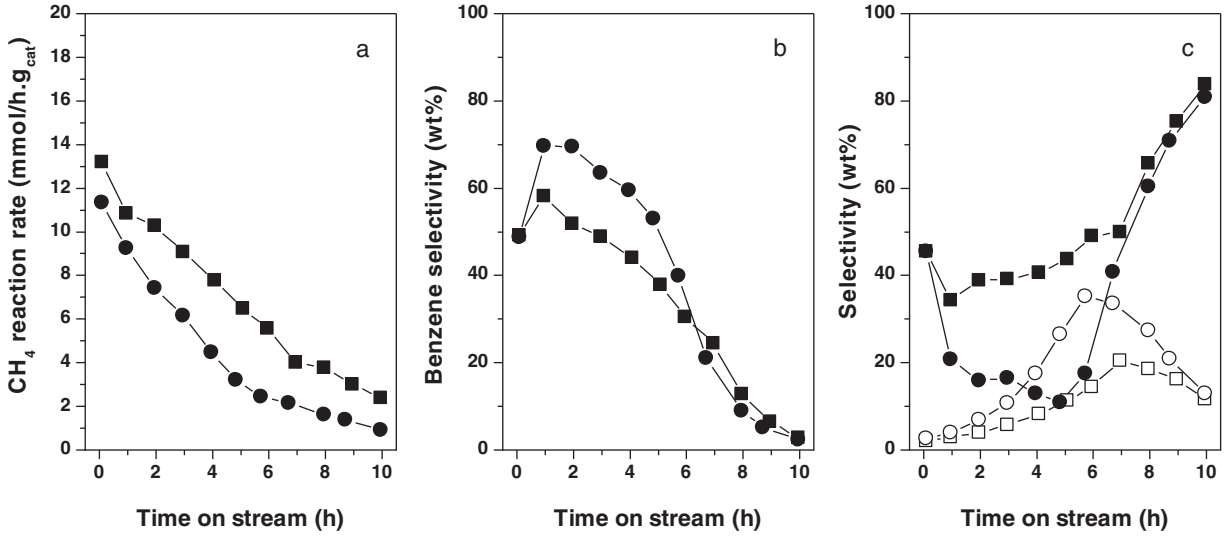

Fig. 1. MDA reaction data for Mo/HZSM-5 (squares) and Mo/HZSM-5(Si) (circles): (a) methane conversion rate, (b) benzene selectivity and (c) coke (closed symbols) and olefin (predominantly ethylene) selectivity (open symbols) as a function of the reaction time (T = 973 K, WHSV = 1.22 h^{-1}).

diameter of 4.0 mm. The catalyst was supported on quartz wool in the isothermal zone of the oven. All gases were fed using thermal mass controllers. The catalyst was activated by increasing the temperature at a rate of 10 K/min to 973 K in a (80/20) (v/v) CH_4/He gas flow of 25 ml/min. The reaction was started by switching the reactor feed to a N_2/CH_4 mixture (5 vol% N_2 in CH_4) at a WHSV of 1.22 h^{-1} (1710 ml CH_4/g_{cat} h at STP conditions). Products were analyzed by an online gas chromatograph (Interscience CompactGC) equipped with three analysis channels for analysis of light gasses (Molsieve 5A, TCD), aromatics (Al_2O_3/KCl, TCD) and light hydrocarbons (Rtx-1, FID).

Nitrogen was used as the internal standard in order to determine the methane conversion (X_{CH4}) and the methane conversion rate (r_{CH4}). The weight-based selectivities and reaction rates of the products ($r_{product}$) were determined using response factors for the various compounds (main products are benzene, toluene, naphthalene, ethylene, ethane, propylene, propane). The coke selectivity (S_{coke}) and the rate of coke formation (r_{coke}) were determined by mass balance considerations.

To follow the deactivation process, samples were recovered after different reaction times by rapidly cooling the reactor under flowing He. The Mo/HZSM-5 samples were then recovered from the reactor in air. This procedure was carried out after activation of the catalyst in CH_4/He and activation in CH_4/He followed by reaction for 5 min, 2 h, 5 h and 10 h. The corresponding samples are denoted by Mo/HZSM-5(act), Mo/HZSM-5(0.08 h), Mo/HZSM-5(2 h), Mo/HZSM-5(5 h) and Mo/HZSM-5(10 h).

3. Results and discussion

3.1. Catalytic activity measurements

Catalytic performance data for Mo/HZSM-5 and Mo/HZSM-5(Si) catalysts in the MDA reaction are shown in Fig. 1. The trends in catalytic activity and selectivity with time on stream were similar for both catalysts. In line with earlier reports [20], the methane conversion rate gradually decreased. After 10 h on stream, nearly all catalytic activity was lost. During reaction, the benzene formation rate strongly decreased. At the same time, the ethylene selectivity increased. These changes point to rapid deactivation of the BAS that convert ethylene to aromatics. It is also seen that, at the initial stages of the reaction, the benzene selectivity was low and the coke selectivity was as high as 50 wt%. In this induction period, part of the methane in the feed is used to convert the Mo-oxide phase into Mo-carbide [20]. This implies that the Mo-oxide precursor was not totally converted to Mo-carbides during heating in CH_4/He. Concomitant with Mo-carbide formation, the coke selectivity decreased and the benzene selectivity increased. The highest benzene selectivity was observed after a reaction time of 1–2 h. The benzene selectivity was higher for Mo/HZSM-5(Si) (75 wt%) than for Mo/HZSM-5 (64 wt%). After 2 h, the benzene selectivity decreased, first relatively slowly, and then more rapidly after 5 h. Especially during the rapid decrease of methane conversion, the ethylene and coke selectivity strongly increased. The coke selectivity for Mo/HZSM-5(Si) was lower compared with its non-silylated counterpart. This difference is in agreement with the coke content of the spent catalysts recovered after 10 h on stream (Table 1). The silylated sample contained less hard coke as determined by TGA. This hard coke is made up from polyaromatic hydrocarbons (PAHs).

Table 1
Carbon analysis of the spent Mo/HZSM-5 and Mo/HZSM-5(Si) catalysts determined by TGA.

Sample	C_{total} (wt%)	C_{MoC} (wt%)	C_{soft} (wt%)	C_{hard} (wt%)
HZSM-5	–	–	–	–
Mo/HZSM-5	–	–	–	–
Mo/HZSM-5(act)	3.7	0.9	2.8	0
Mo/HZSM-5(0.08 h)	3.7	0.7	3.0	0
Mo/HZSM-5(2 h)	7.8	0	4.0	3.8
Mo/HZSM-5(5 h)	11.3	0	4.1	7.2
Mo/HZSM-5(10 h)	14.2	0	3.8	10.4
Mo/HZSM-5(Si)	–	–	–	–
Mo/HZSM-5(Si,act)	4.7	4.1	0.6	0
Mo/HZSM-5(Si,2 h)	9.3	0	3.3	6.0
Mo/HZSM-5(Si,10 h)	12.3	0	2.5	9.8

3.2. Catalyst characterization

The XRD patterns of the fresh catalysts show that the introduction of Mo did not strongly affect the crystallinity of the zeolites (Table 2). There are no indications for the presence of large MoO_3 crystallites in the diffractograms. The textural properties of the zeolite catalysts are listed in Table 2. The decrease in the micropore volume upon introduction of Mo indicates that a fraction of the Mo phase is located in the zeolite micropores [20]. Activation in a mixture of CH_4/He at 973 K led to a decrease of the

Table 2
Textural properties of fresh and spent Mo/HZSM-5 and Mo/HZSM-5(Si).

Sample	V_{micro} (cm^3/g)	V_{meso} (cm^3/g)	S_{micro} (m^2/g)	S_{meso} (m^2/g)	S_{BET} (m^2/g)	XRD crystallinity (%)
HZSM-5	0.13	0.02	246	10	251	100
Mo/HZSM-5	0.10	0.03	204	14	244	93
Mo/HZSM-5(act)	0.07	0.04	130	18	164	–
Mo/HZSM-5(0.08 h)	0.07	0.03	135	19	179	–
Mo/HZSM-5(2 h)	0.07	0.04	140	22	196	–
Mo/HZSM-5(5 h)	0.04	0.023	87	12	115	–
Mo/HZSM-5(10 h)	0	0.02	3	7	8	–
Mo/HZSM-5(Si)	0.06	0.02	131	11	162	90
Mo/HZSM-5(Si,act)	0.05	0.03	105	15	137	–
Mo/HZSM-5(Si,2 h)	0.03	0.03	6	18	104	–
Mo/HZSM-5(Si,10 h)	0.00	0.01	5	5	4	–

micropore volume, which may be due to formation of Mo-carbide species and the deposition of carbonaceous species close to these Mo-carbides [10]. The catalysts recovered directly after activation and after 5 min and 2 h on stream all had comparable micropore volume ($V_{micro} \approx 0.07\ cm^3/g$). This suggests that the rate of carbon deposition during the first 2 h of the reaction was relatively low. Samples recovered after 5 h and 10 h had much lower micropore volumes of 0.04 cm^3/g and 0 cm^3/g, respectively. The decrease shows that substantial amounts of coke formed inside the micropores or at the external surface, blocking the micropore entrances during the second stage of the reaction. We verified for spent Mo/HZSM-5 that the complete loss in micropore volume was not due to the amorphization of the zeolite; after a reaction time of 10 h, the zeolite crystallinity remained at 64%.

The Al speciation in the fresh and spent zeolites was characterized by ^{27}Al MAS NMR spectroscopy. The weight-normalized ^{27}Al MAS NMR spectrum of HZSM-5 (Fig. 2) contains a dominant feature at $\delta = 55$ ppm (δ, chemical shift) due to framework Al (FAl) atoms and a smaller feature at $\delta = 0$ ppm due to extraframework Al (EFAl) species. Modification of HZSM-5 with Mo (Mo/HZSM-5) led to a decrease and broadening of the FAl signal caused by the proximity of cationic Mo-oxo complexes that replace the protons [21]. Two weak features at $\delta = -11$ ppm and $\delta = 14$ ppm are due to EFAl species in the form of $Al_2(MoO_4)$. The NMR spectra of the spent samples show a decreasing FAl content for increasing MDA reaction time. Although the weak shoulder at $\delta = 30$ ppm due to distorted four-coordinated or five-coordinated Al species [22] increased slightly, the decrease in FAl content is not paralleled by an increase in EFAl content. The increasing amount of NMR-invisible Al may be related to framework damage occurring during the MDA reaction. It is however at odds with the remaining crystallinity of the spent Mo/HZSM-5(10 h) sample. Another explanation is that rehydration of the spent samples before the ^{27}Al NMR measurements may be incomplete because of the decreased micropore accessibility. The resulting asymmetric Al coordination environments can in principle also explain the decreased NMR-visibility of the Al atoms.

Conventional characterization of the surface acidity by IR spectroscopy of the activated and spent samples was not possible, because the samples were black due to carbon laydown. We used the low-temperature isotopic exchange reaction between perdeuterobenzene and benzene to probe the Brønsted acidity of the activated and spent Mo/HZSM-5 catalysts. The isotopic exchange reaction between C_6H_6 and C_6D_6 can be catalyzed by BAS at relatively low temperatures [23]. This reaction has been earlier successfully employed in order to determine the concentration of BAS of zeolites, clays and amorphous silica–alumina [24–26]. We used the rate of C_6H_5D formation at a temperature of 313 K as a measure for the number of BAS. This isotopomer is the main reaction product of isotopic exchange reaction of C_6H_6, because C_6H_6 was present in tenfold excess to C_6D_6 in the reactant feed mixture. The absolute reaction rates and the relative reaction rates compared with the parent HZSM-5 zeolite are given in Table 3. The reaction rate of Mo/HZSM-5 was only slightly lower than that of the parent HZSM-5 zeolite, consistent with the relatively small decrease in the bridging hydroxyl density upon Mo introduction as probed by IR spectroscopy [17,27,28]. Activation in methane resulted in a significant decrease of the Brønsted acidity. Although it is usually assumed that some BAS are regenerated by the carburization of cationic Mo-oxo complexes, we found that the overall acidity decreased further during the carburization step. Together with the textural data, we conclude that blockage of the micropores was the main cause of the decreased acidity. The H/D exchange data show that the accessible acidity was lower after prolonged reaction. After 5 min on stream, already half of the acid sites of the fresh Mo/HZSM-5 were not involved in the H/D exchange reaction anymore. The acidity gradually decreased for prolonged reaction times and, after 10 h on stream, the accessible acidity was nearly completely lost.

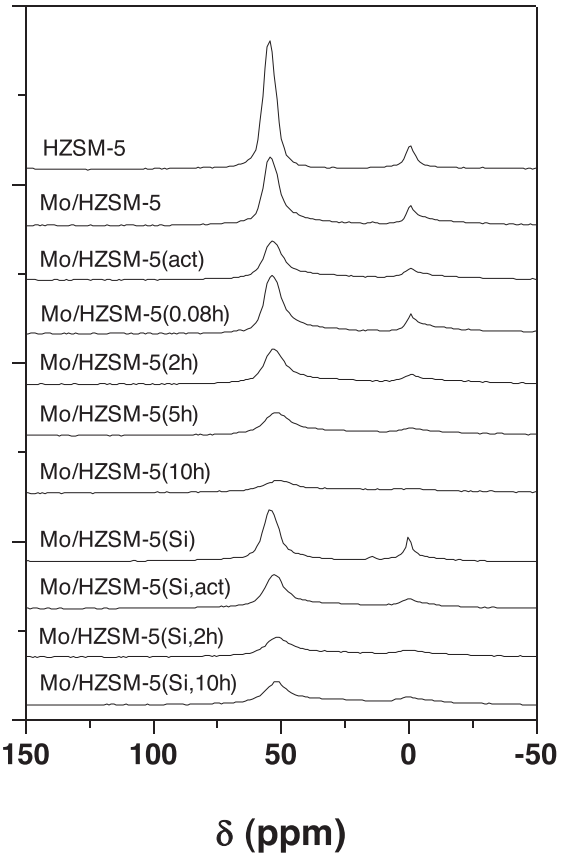

Fig. 2. ^{27}Al MAS NMR spectra of the parent, activated and spent Mo/HZSM-5 catalysts.

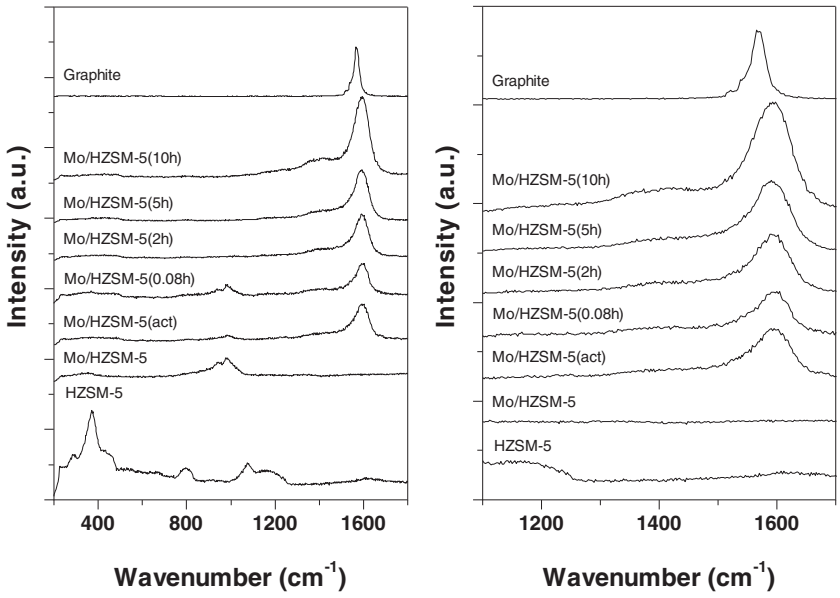

Fig. 3. UV Raman spectra ($\lambda_{excitation}$ = 244 nm) of the parent, activated and spent Mo/HZSM-5 catalysts.

Table 3
Physico-chemical properties of fresh and spent Mo/HZSM-5 and Mo/HZSM-5(Si).

Sample	Mo/Al[a]	I_{FAl}[b] (%)	$r_{H/D}$[c] (mmol/min g_{cat})	Normalized $r_{H/D}$[d]
HZSM-5	–	100	1.27	1
Mo/HZSM-5	0.39	53	1.18	0.92
Mo/HZSM-5(act)	0.39	37	0.79	0.62
Mo/HZSM-5(0.08 h)	0.39	40	0.61	0.46
Mo/HZSM-5(2 h)	0.39	34	0.36	0.28
Mo/HZSM-5(5 h)	0.39	23	0.14	0.11
Mo/HZSM-5(10 h)	0.39	11	0	0
Mo/HZSM-5(Si)	–	42	–	–
Mo/HZSM-5(Si,act)	–	23	–	–
Mo/HZSM-5(Si,2 h)	–	14	–	–
Mo/HZSM-5(Si,10 h)	–	15	–	–

[a] Atomic Mo/Al ratio as determined by ICP-OES analysis.
[b] FAl concentration references to HZSM-5 as determined by ^{27}Al MAS NMR spectroscopy.
[c] Isotopic exchange rate.
[d] Relative isotopic exchange rate normalized to HZSM-5.

The acidity decrease strongly correlates with the loss in micropore volume as determined by Ar physisorption.

The Mo speciation in the external surface region of the zeolite crystals was investigated by XPS. Table 4 collects the XPS results including reference binding energies for various Mo species taken from literature [29]. It is difficult to discern between metallic Mo and highly dispersed Mo_2C (Mo_2C_{small}), because these species have nearly similar binding energies [30]. Wang et al. mentioned that carburization of MoO_3 to Mo_2C particles is thermodynamically favored over full reduction of Mo species to metallic Mo under MDA conditions [30]. The Mo speciation is given in Table 4. The parent Mo/HZSM-5 zeolite mainly comprised MoO_3. Upon activation in methane, MoO_3 was almost completely converted into highly dispersed Mo_2C. Small amounts of MoO_2 and large Mo_2C particle (Mo_2C_{large}) were also observed. After 5 min of reaction (Mo/HZSM-5(0.08)), the oxidation degree of the Mo phase was higher than directly after carburization. A likely explanation is that the replacement of the diluted methane feed used for pre-carburization by the pure methane reactant feed led to a much higher carburization rate of the remaining oxides and formation of water. The formation of water may result in re-oxidation of some of the Mo-carbides at the surface. After prolonged reaction, the amount of low-dispersed Mo_2C particles has increased at the expense of highly dispersed Mo_2C particles, pointing to slow sintering of the initially highly dispersed Mo_2C particles during the MDA reaction. The XPS data show that, at the same time, the Si/C and Al/C ratios in the surface region decreased (Table 4). We interpret this in terms of the formation of a carbonaceous layer around the zeolite that separates the Mo-phase from the zeolite surface.

The nature of the Mo phase and carbonaceous deposits in the fresh, activated and spent catalysts was investigated by UV Raman spectroscopy (Fig. 3). The Raman signal upon 244 nm excitation mostly derives from the species present at the external surface of

Table 4
Mo and C speciation in surface region of spent Mo/HZSM-5 and Mo/HZSM-5(Si) catalysts as determined by XPS.[a]

Sample	MoO_3 (%)	MoO_2 (%)	Mo_2C_{small} (%)	Mo_2C_{large} (%)	Atomic ratios		
					Si/Al	Al/C	Si/C
Mo/HZSM-5	100	0	0	0	18.5	0.43	1.64
Mo/HZSM-5(act)	1	15	65	18	19.3	0.23	0.92
Mo/HZSM-5(0.08 h)	16	32	27	25	19.4	0.13	0.53
Mo/HZSM-5(2 h)	11	30	23	37	20.8	0.08	0.35
Mo/HZSM-5(5 h)	10	30	5	55	19.3	0.05	0.19
Mo/HZSM-5(10 h)	7	27	11	55	22.3	0.02	0.09
Mo/HZSM-5(Si)	100	0	0	0			
Mo/HZSM-5(Si,act)	33	39	4	23	22.2	0.12	0.52
Mo/HZSM-5(Si,2 h)	15	35	19	31	22.1	0.09	0.43
Mo/HZSM-5(Si,10 h)	1	29	11	60	22.0	0.004	0.14

[a] Binding energy of Mo species from Ref. [29]: MoO_3: 232.7 eV; MoO_2: 229.8 eV; Mo_2C_{small}: 227.6 eV; Mo_2C_{large}: 228.0 eV.

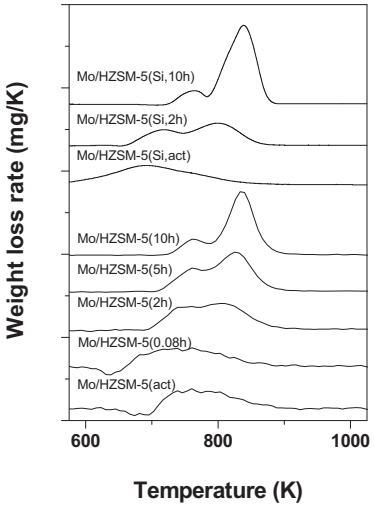

Fig. 4. Weight-loss curves of activated and spent Mo/HZSM-5 zeolites.

the zeolite crystals [12]. The Raman spectrum of HZSM-5 shows bands that are typical for MFI zeolite [18]. The most prominent band at 380 cm^{-1} can be assigned to the double-five-ring vibration of the MFI framework. In Mo/HZSM-5, the intensity of this band is very low, which is caused by the presence of Mo-oxo species at the external zeolite surface [31]. Compared with HZSM-5, the spectrum of Mo/HZSM-5 contains additional bands at 280 cm^{-1}, 336 cm^{-1}, 821 cm^{-1} and 995 cm^{-1}, which can be attributed to α-MoO_3 [32–34,8]. Upon activation in methane, the α-MoO_3 signals disappeared as a result of carburization of the Mo-oxides [35]. New broad bands appear at ~1400 cm^{-1} and ~1600 cm^{-1}. A closer look at this region (right panel of Fig. 3) shows that the band at 1600 cm^{-1} shifted toward lower wavenumbers for prolonged reaction times. Li et al. have assigned Raman bands in this region to various types of carbon [36]. PAHs and graphitic carbon give rise to bands at 1595 cm^{-1} and 1585 cm^{-1}, respectively [36]. Accordingly, we attribute the spectral changes to the formation of increasing amounts of PAHs and graphitic carbon during the MDA reaction. The shoulders visible at 1610 cm^{-1} and 1560 cm^{-1} relate to adsorbed naphthalene molecules and to conjugated olefinic species, respectively [36]. The broad band at 1385 cm^{-1} is typical for coke formed from olefinic precursors. The band originally positioned at 1385 cm^{-1}, which shifted toward 1365 cm^{-1} after prolonged reaction; is characteristic for graphitic carbon [36]. In summary, the Raman spectra point to the formation of significant amounts of PAHs and graphitic carbon in the spent samples.

TGA was employed to characterize the carbonaceous deposits on the spent catalysts (Fig. 4). Three types of carbon were distinguished as a function of the calcination temperature during TGA in artificial air. These include relatively light carbonaceous species associated with Mo-carbides (C_{MoC}, ~693 K), soft coke (C_{soft}, ~753 K) and hard coke (C_{hard}, ~813 K). Soft coke is thought to be amorphous in nature and likely formed in the proximity of Mo-carbide particles [37,38]. Hard coke is mainly comprised of PAHs formed by reactions of olefins on BAS located at the external surface of the zeolite. Table 1 lists the results of deconvolution of the TGA curves in Fig. 4. The catalysts recovered after the activation step and after 5 min reaction (Mo/HZSM-5(0.08)) contained about 25% C_{MoC} and 75% C_{soft} and very little hard coke. The total amount of carbon was similar for these samples. Longer reaction times led to a significant increase of the total carbon content, almost exclusively in the form of hard coke.

We used transmission electron microscopy to study the dispersion of the Mo-oxide/carbide phase in more detail. Bright-field TEM images are shown in Fig. 5; Fig. 6 reports HAADF-STEM images. For fresh Mo/HZSM-5, a few large MoO_3 particles with sizes up to 100 nm are visible at the external zeolite surface. As the XRD patterns did not contain evidence for such large MoO_3 particles, we conclude that the amount of such large particles is relatively small. Activation in methane converted the Mo-oxide particles to small Mo_2C particles (Fig. 5b). Only a relatively small amount of Mo_2C particles larger than 10 nm are visible in the EM images. Close inspection of the images reveals that an amorphous carbon layer has formed at the external surface of the zeolite crystals. Some of the Mo_2C particles are separated from the zeolite crystal by this carbonaceous layer. After activation, also some carbon nanotubes are visible in line with earlier findings [39]. The TEM images of the catalyst recovered after 2 h of reaction (Fig. 5c) showed a much lower density of small-sized Mo_2C particles. Clearly, the Mo-carbide particles sinter during the MDA reaction. After 2 h, the amorphous carbon layer covers a significant fraction of the external zeolite surface. Compared with Mo/HZSM-5(act), more Mo_2C particles were seen to be separated from the zeolite surface by this carbonaceous layer. After 10 h on stream, the carbonaceous layer was much thicker; it is difficult to discern the external surface of the zeolite (Fig. 5d). In this sample, the Mo_2C phase was present as relatively large particles. The images taken in STEM-HAADF mode (Fig. 6) serve to illustrate the gradual transformation of the Mo-carbide phase from highly dispersed particles in the activated catalyst toward large agglomerated particles after 10 h reaction. It supports the conclusion that the dispersion of the Mo-oxide phase is initially very high. Upon carburization, they slowly sinter during the MDA reaction; this process is accelerated by the detachment of these particles from the external zeolite surface support, which is caused by the carbonaceous layer.

We also characterized some of the spent Mo/HZSM-5(Si) catalysts. The results were qualitatively similar to those obtained for the spent Mo/HZSM-5 samples. A gradual decrease in the micropore volume (Table 2) was observed with reaction time. The micropore volume of the sample retrieved after 10 h reaction was also negligible for the silylated zeolite catalyst. The FAl content as determined by NMR spectroscopy also decreased with the progressing reaction. For silylated Mo/HZSM-5, XPS data point out the formation of a carbonaceous layer around the zeolite crystals. TGA confirms that PAHs are the main compounds in the carbonaceous layer formed around the zeolite crystals. Although the general trends are similar, some subtle differences can be noted between Mo/HZSM-5 and Mo/HZSM-5(Si). The micropore volumes for the spent Mo/HZSM-5(Si) catalysts were lower than those of the Mo/HZSM-5 analogs. This is due to the improved spreading of the Mo phase upon silylation [17]. Activated Mo/HZSM-5(Si) contained more MoO_3 and MoO_2 in comparison with Mo/HZSM-5(act). This difference suggests slower carburization of the Mo-oxide precursor in silylated Mo/HZSM-5, possibly due to the increased interaction of the Mo-oxide precursor with the zeolite surface. TGA of the carbonaceous deposits revealed a relative large amount of soft coke after activation of Mo/HZSM-5(Si)). Combined with the XPS and textural analysis data, these findings support the conclusion that the Mo dispersion upon the silylation treatment of Mo/HZSM-5 was improved. The overall carbon content of the spent Mo/HZSM-5(Si) after 10 h was lower compared to that of the non-silylated analog. The initial total carbon content of Mo/HZSM-5(Si) was higher than that of Mo/HZSM-5. We believe that the amount of carbon formed due to undesired side-reactions in Mo/HZSM-5(Si,2 h) is overestimated by the TGA analysis. This is caused by the encapsulation of MoC_x with a layer of carbonaceous deposits. As these deposits have to be oxidized (at higher temperature) before the MoC_x particles can be oxidized, the TGA curves cannot be used to determine the content of the Mo-carbide particles. In this way, the amount of coke

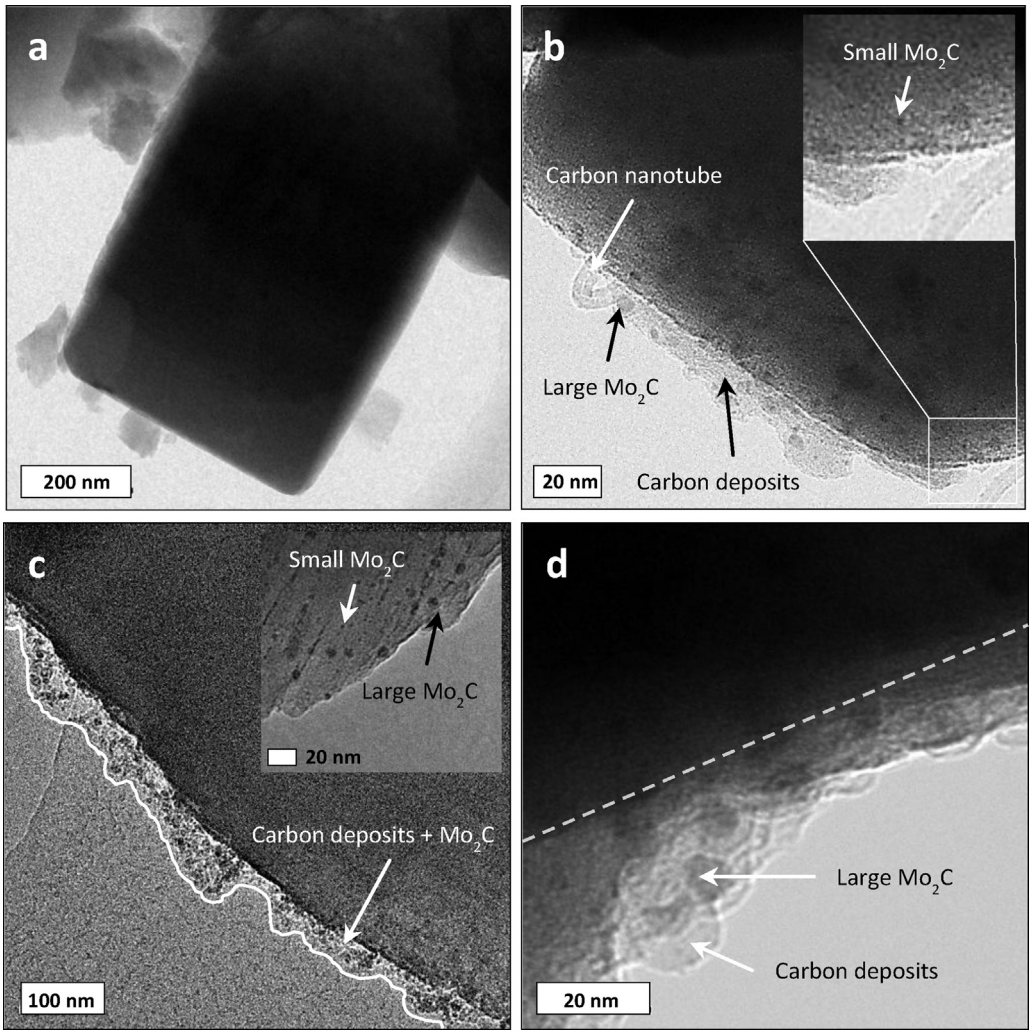

Fig. 5. TEM images of (a) Mo/HZSM-5, (b) Mo/HZSM-5(act), (c) Mo/HZSM-5(2 h) and (d) Mo/HZSM-5(10 h).

is overestimated and the amount of MoC_x is underestimated. Subtracting the initial C_{MoC} content from the C_{total} in the spent catalysts recovered after 2 h in the MDA reaction indicates that less carbon deposits were formed on Mo/HZSM-5(Si,2 h) (9.3–4.1 = 5.2 wt%) compared with Mo/HZSM-5(2 h) (7.8–0.9 = 6.9 wt%).

3.3. Deactivation mechanism

This study investigated the deactivation of the Mo/HZSM-5 catalyst in the bifunctional MDA reaction. It is generally assumed that the Mo-carbide phase converts methane into ethylene and hydrogen. The olefins are then reacted on the BAS to aromatic compounds. The main focus of the present investigation was on the changes of the catalyst upon activation and during reaction that lead to catalyst deactivation. An important finding of the present study is that a thick carbonaceous layer is formed at the external zeolite surface. This layer blocks the access of the olefinic intermediates to the acid sites. In addition, it leads to the detachment of the Mo-carbide particles from the zeolite surface, thereby accelerating their sintering. While the lower accessibility of the acid sites mainly affects the product distribution, the sintering of the Mo-carbide phase leads to decreased methane conversion rates. During catalyst preparation, Mo modification of the parent zeolite (Fig. 7a) leads to the migration of a small fraction of mobile Mo-oxo species into the micropore space during the calcination step (Fig. 7b). Most of the Mo-oxo species remain at the external surface, predominantly in the form of highly dispersed particles, but also as some larger MoO_3 crystallites. Upon activation in methane, the Mo-oxide carburizes (Fig. 7c). The resulting Mo-carbide (MoC_x) particles are mainly present in highly dispersed form at the external surface and inside the micropores. During the carburization process, the micropore volume became lower, which may be attributed to the growth of the Mo-carbide species in the micropores as well as the formation of amorphous polyolefinic (soft coke) associated with Mo-carbides. At the external surface, a small amount of PAHs (hard coke) forms. The BAS located at the external surface are most likely involved in the formation of these hard coke deposits. We speculate that also silanol groups may be implicated in oligomerization reactions of unsaturated intermediates at the very high temperatures used for the MDA reaction.

During the first 2 h of reaction, the micropore volume did not substantially change. After 2 h, part of the highly dispersed Mo_2C particles at the external surface agglomerated into larger particles as evidenced by TEM measurements (Fig. 7d). Agglomeration of the MoC_x phase may be attributed to the decreased interaction of the particles with the external zeolite surface. This is caused by the formation of a carbon layer at the external surface that separates the MoC_x particles from the zeolite external surface as seen in the TEM images. It has been reported that large MoC_x particles

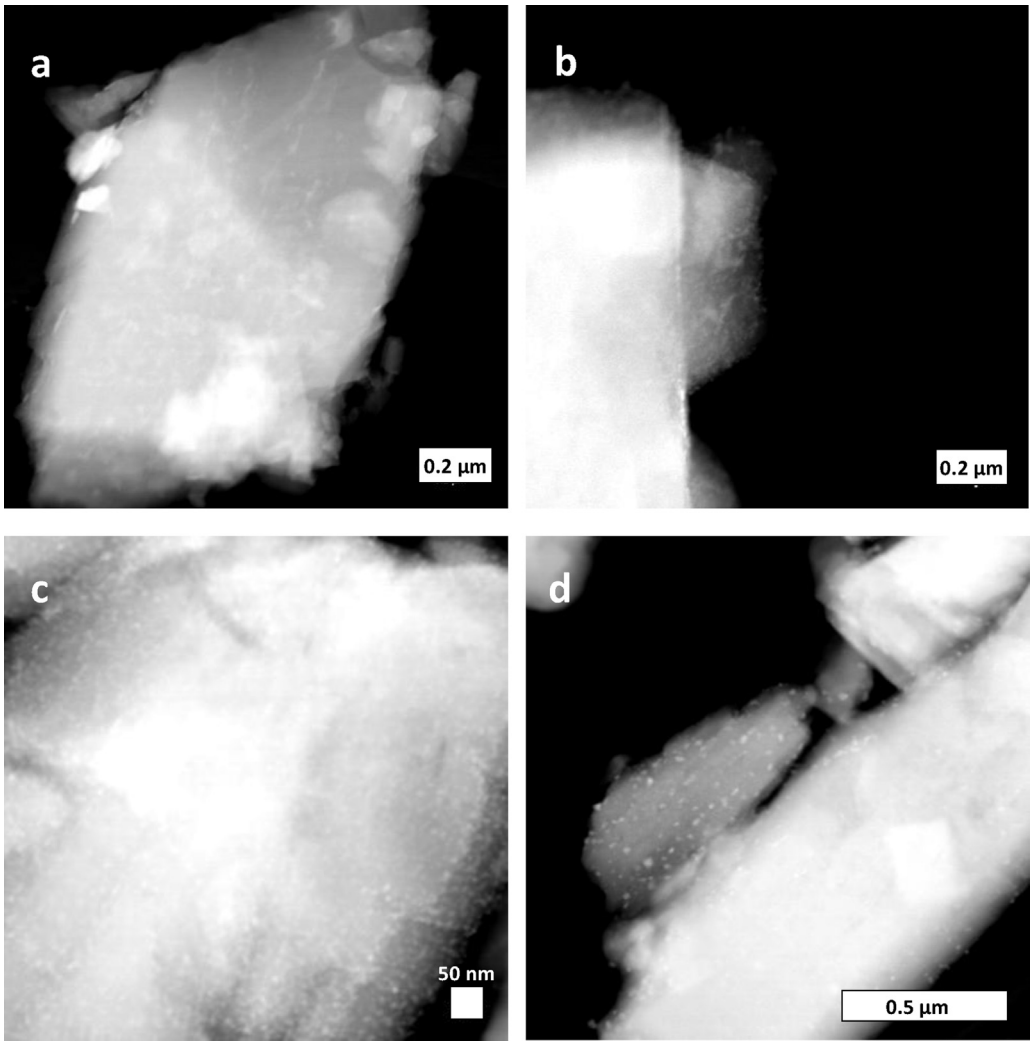

Fig. 6. STEM-HAADF images of (a) Mo/HZSM-5, (b) Mo/HZSM-5(act), (c) Mo/ZSM-5(2 h) and (d) Mo/HZSM-5(10 h).

are undesired, because they exhibit high selectivity toward coke and, accordingly, accelerate deactivation [39]. Based on our results, we argue that the loss in MoC_x dispersion is the main reason for the decreased methane conversion rate observed in the catalytic performance data.

After 2 h, the PAHs layer rapidly grows over the external zeolite surface (Fig. 7e and f) and, in this way, lowers the micropore volume. Consequently, the amount of BAS accessible to olefinic intermediates is decreased. As the formation of hard coke correlates well with the loss in micropore volume, we attribute the decrease

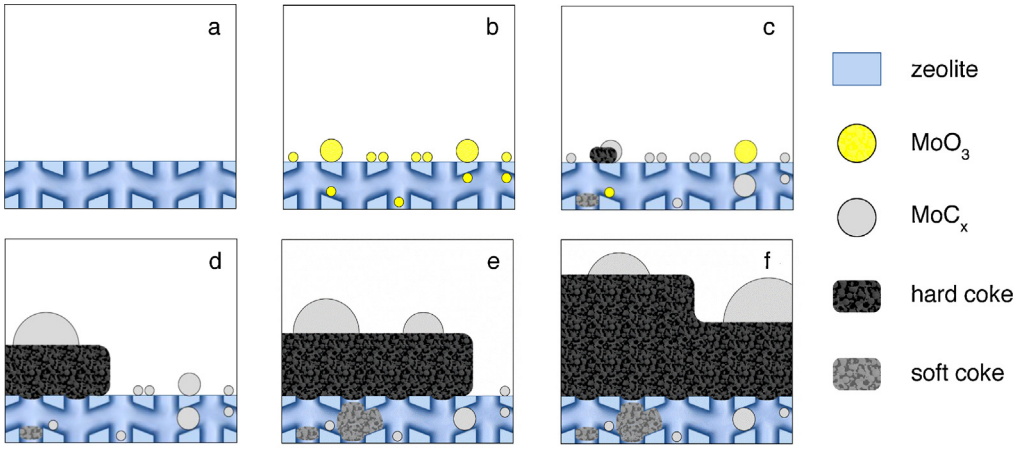

Fig. 7. Schematic representation of the state of Mo/HZSM-5 during its life as an MDA catalyst. The cartoons represent (a) parent HZSM-5, (b) Mo/HZSM-5, (c) Mo/HZSM-5(act), (d) Mo/HZSM-5(2 h), (e) Mo/HZSM-5(5 h) and (f) Mo/HZSM-5(10 h).

in aromatics selectivity with time on stream to the decreased accessibility of the shape-selective BAS located in the micropores. Agglomeration of MoC_x particles and formation of soft coke inside the micropores may also contribute to the decreasing pore volume. After 10 h on stream, the thickness of the polyaromatic carbon layer has grown to 20 nm (Fig. 7f). It leads to the nearly complete inaccessibility of the micropores.

In summary, we attribute catalyst deactivation to the formation of a PAHs hard coke layer at the external zeolite surface. It leads to blockage of the micropores and, accordingly, to decreased accessibility of the BAS inside the micropores. These sites are responsible for the formation of benzene; their lower accessibility explains the decrease in benzene selectivity. The formation of the carbon layer leads to sintering of the highly dispersed MoC_x particles at the external surface into larger ones. As a result of the decreasing MoC_x dispersion, the methane conversion rate decreases. All of these changes also occur in the silylated Mo/HZSM-5 catalyst. The main benefit of the silylation treatment is the lower rate of formation of PAHs at the external surface due to the deactivation of the external acidity.

4. Conclusions

The deactivation of Mo/HZSM-5 catalysis in the MDA reaction was investigated. The parent zeolite, the Mo-modified zeolite catalyst and activated and spent catalysts were characterized in detail for their textural properties, the dispersion and location of the Mo-oxide/carbide phase and the nature of the carbonaceous deposits. After carburization of the Mo-oxide phase, optimum performance in terms of benzene yield is reached. The formation of a carbonaceous layer consisting of PAHs at the external surface decreases the accessibility of the BAS in the zeolite micropores. Simultaneously, this carbonaceous layer lowers the interaction of the Mo-carbide particles with the external zeolite surface. As a consequence, the Mo-carbide particles sinter, which explains the decreased methane conversion rate. The lower Brønsted acidity shifts the selectivity from benzene to unsaturated olefinic intermediates. The hard coke layer at the external surface is due to acid sites that can be partially deactivated by silylation.

References

[1] P.C.A. Bruijnincx, B.M. Weckhuysen, Angew. Chem. Int. Ed. 52 (2013) 11980–11987.
[2] G.J. Kramer, M. Haigh, Nature 462 (2009) 568–569.
[3] British Petroleum Company, BP Statistical Review of World Energy, British Petroleum Co., London, 2013, pp. 20.
[4] H. Rogers, Oxford Rev. Econ. Pol. 27 (2011) 117–143.
[5] L. Wang, L. Tao, M. Xie, G. Xu, Catal. Lett. 21 (1993) 35–41.
[6] B.S. Liu, J.W.H. Leung, L. Li, C.T. Au, A.S.-C. Cheung, Chem. Phys. Lett. 430 (2006) 210–214.
[7] J. Bai, S. Liu, S. Xie, L. Xu, L. Lin, Catal. Lett. 90 (2003) 123–130.
[8] J. Bai, S. Lie, S. Xie, L. Xu, L. Lin, React. Kinet. Catal. Lett. 82 (2004) 279–286.
[9] S. Li, M.A. d, Q. Kan, P. Wu, Y. Peng, C. Zhang, M. Li, Y. Fu, J. Shen, T. Wu, X. Bao, React. Kinet. Catal. Lett. 70 (2000) 349–356.
[10] D. Ma, Y. Shu, M. Cheng, Y. Xu, X. Bao, J. Catal. 194 (2000) 105–114.
[11] E.V. Matus, I.Z. Ismagilov, O.B. Sukhova, V.I. Zaikovskii, L.T. Tsikoza, Z.R. Ismagilov, Ind. Eng. Chem. Res. 46 (2007) 4063–4074.
[12] F. Fan, K. Sun, Z. Feng, H. Xia, B. Han, Y. Lian, P. Ying, C. Li, Chem. Eur. J. 15 (2009) 3268–3276.
[13] T. Behrsing, H. Jaeger, J.V. Sanders, Appl. Catal. 54 (1989) 289–302.
[14] W.P. Ding, G.D. Meitzner, E. Iglesia, J. Catal. 206 (2002) 14–22.
[15] H.M. Liu, Y. Li, W.J. Shen, X.H. Bao, Y.D. Xu, Catal. Today 93–95 (2004) 65–73.
[16] S. Kikuchi, R. Kojima, H.T. Ma, J. Bai, M. Ichikawa, J. Catal. 242 (2006) 349–356.
[17] C.H.L. Tempelman, V.O. de Rodrigues, E.H.R. van Eck, P.C.M.M. Magusin, E.J.M. Hensen, Micropor. Mesopor. Mater. 203 (2015) 259–273.
[18] J. Chen, Z. Feng, P. Ying, C. Li, J. Phys. Chem. B 108 (2004) 12669–12676.
[19] B.C. Lippens, J.H. de Boer, J. Catal. 4 (1965) 319–323.
[20] Y. Shu, D. Ma, L. Xu, Y. Xu, X. Bao, Catal. Lett. 70 (2000) 67–73.
[21] J.-P. Tessonnier, B. Louis, S. Rigolet, M.J. Ledoux, C. Pham-Huu, Appl. Catal. A 336 (2008) 79–88.
[22] R.K. Sato, P.F. McMillan, P. Dennison, R. Dupree, J. Phys. Chem. 95 (1991) 4483–4489.
[23] R.A. van Santen, G.J. Kramer, Chem. Rev. 95 (1995) 637–660.
[24] L.W. Beck, T. Xu, J.B. Nicholas, J.F. Haw, J. Am. Chem. Soc. 117 (1995) 11594–11595.
[25] E.J.M. Hensen, D.G. Poduval, V. Degirmenci, D.A.J.M. Ligthart, W. Chen, F. Maugé, M.S. Rigutto, J.A.R. van Veen, J. Phys. Chem. C 114 (2010) 8363–8374.
[26] E.J.M. Hensen, D.G. Poduval, D.A.J.M. Ligthart, J.A.R. van Veen, M.S. Rigutto, J. Phys. Chem. C 114 (2010) 8363–8374.
[27] R.W. Borry III, Y.H. Kim, A. Huffsmith, J.A. Reimer, E. Iglesia, J. Phys. Chem. B 103 (1999) 5787–5796.
[28] J.-P. Tessonnier, B. Louis, S. Walspruger, J. Sommer, M.-J. Ledoux, C. Pham-Huu, J. Phys. Chem. B 110 (2006) 10390–10395.
[29] F. Solymosi, J. Cserényi, A. Szöke, T. Bánsági, A. Oszkó, J. Catal. 165 (1997) 150–161.
[30] D. Wang, J.H. Lunsford, M.P. Rosynek, Top. Catal. 3 (1996) 289–297.
[31] C. Li, J. Catal. 216 (2003) 203–212.
[32] G. Mestl, T.K.K. Srinivasan, Catal. Rev. Sci. Eng. 40 (1998) 451–570.
[33] W. Li, G.D. Meitzner, R.W. Borry III, E. Iglesia, J. Catal. 191 (2000) 373–383.
[34] A.M. Rzehvskii, P. Choi, F.H. Ribeiro, R.J. Gulotty Jr., M.M. Olken, Catal. Lett. 73 (2001) 187–191.
[35] D. Ma, Y. Shu, X. Han, X. Liu, Y. Xu, X. Bao, J. Phys. Chem. B 105 (2001) 1786–1793.
[36] C. Li, P.C. Stair, Catal. Today 33 (1997) 353–360.
[37] B.S. Liu, L. Jiang, H. Sun, C. Au, T, Appl. Surf. Sci. 253 (2007) 5092–5100.
[38] S. Qu, B. Yang, Catal. Today 98 (2004) 639–645.
[39] F. Solymosi, A. Szöke, J. Cserényi, Catal. Lett. 39 (1996) 157–161.